

## Antibacterial CATH-2 Peptide Coating to Prevent Bone Implant-Related Infection

Keikhosravani, Pardis; Jahanmard, Fatemah; Bollen, Tim ; Nazmi, Kamran; Veldhuizen, Edwin J. A. ; Gonugunta, P.; Ravi Anusuyadevi, P.; van der Wal, Bart C.H.; Vogely, Charles; Bikker, Floris J.

**DOI**

[10.1002/admt.202300500](https://doi.org/10.1002/admt.202300500)

**Publication date**

2023

**Document Version**

Final published version

**Published in**

Advanced Materials Technologies

**Citation (APA)**

Keikhosravani, P., Jahanmard, F., Bollen, T., Nazmi, K., Veldhuizen, E. J. A., Gonugunta, P., Ravi Anusuyadevi, P., van der Wal, B. C. H., Vogely, C., Bikker, F. J., Taheri, P., Weinans, H. H., & Yavari, S. A. (2023). Antibacterial CATH-2 Peptide Coating to Prevent Bone Implant-Related Infection. *Advanced Materials Technologies*, 8(18), Article 2300500. <https://doi.org/10.1002/admt.202300500>

**Important note**

To cite this publication, please use the final published version (if applicable).  
Please check the document version above.

**Copyright**

Other than for strictly personal use, it is not permitted to download, forward or distribute the text or part of it, without the consent of the author(s) and/or copyright holder(s), unless the work is under an open content license such as Creative Commons.

**Takedown policy**

Please contact us and provide details if you believe this document breaches copyrights.  
We will remove access to the work immediately and investigate your claim.

# Antibacterial CATH-2 Peptide Coating to Prevent Bone Implant-Related Infection

Pardis Keikhosravani, Fatemeh Jahanmard, Tim Bollen, Kamran Nazmi, Edwin J. A. Veldhuizen, Prasad Gonugunta, Prasaanth Ravi Anusuyadevi, Bart C.H. van der Wal, Charles Vogely, Floris J. Bikker, Peyman Taheri, Harrie Weinans, and Saber Amin Yavari\*

The development of antibacterial coatings is a promising approach to preventing biofilm formation and reducing the overuse of systemic antibiotics. However, widespread antibiotic use has resulted in antibiotic-resistant bacteria, limiting the efficacy of antibiotic-based coatings. Herein, an antibacterial coating is developed by layer-by-layer (LbL) assembly of two polymers namely PDLG (poly (D,L-lactide-co-glycolide)) and gelatin methacryloyl (GelMA) while chicken cathelicidin-2 (CATH-2), a cationic and amphipathic peptide, is loaded between these polymer layers. The electrospray method is used to apply the coatings to achieve efficient peptide loading and durability. The CATH-2 bactericidal concentration ranges are first identified, followed by a study of their cytotoxicity to human mesenchymal stem cells (hMSCs) and macrophage cell lines. Later, different LbL electrospray coating assemblies loaded with the optimal peptide concentration are sought. Various coating strategies are investigated to identify an LbL coating that exhibits prolonged and biocompatible CATH-2 release. The resulting CATH-2-coated titanium surfaces exhibit strong antibacterial activity against both *Staphylococcus aureus* and *Escherichia coli* bacteria for 4 days and are biocompatible with hMSCs and macrophage cells. This coating can be considered as a versatile delivery system platform for the delivery of CATH-2 peptides while avoiding cytotoxicity, particularly for the prevention of infections associated with implants.

## 1. Introduction

Implant-related infection (IRI) is a major issue with surgical implants, such as hip replacements, dental implants, and other medical devices. Bacteria colonize the implant and form biofilm, leading to a difficulty in treating infection with potential implant failure and a long patient recovery time.<sup>[1]</sup> *Staphylococcus aureus* is one of the bacteria most frequently associated with bone implant infections and biofilm formation.<sup>[2]</sup> In some cases, one or two-step revision surgery is required to remove and replace an infected implant.<sup>[3]</sup> It appears that at the stage of initial bacteria surface adherence only a small window of opportunity exists for immune cells or other therapeutic strategies to prevent biofilm development. Once the biofilm is formed, biofilm-residing bacteria require approximately 1000 times higher antibiotic concentrations than planktonic bacteria, yet lead to toxic side effects.<sup>[4,5]</sup> Hence, IRI management should focus on prevention.


P. Keikhosravani, F. Jahanmard, T. Bollen, B. C. van der Wal, C. Vogely, H. Weinans, S. Amin Yavari  
Department of Orthopedics  
University Medical Center Utrecht  
Utrecht 3508 GA, The Netherlands  
E-mail: s.aminyavari@umcutrecht.nl

F. Jahanmard  
Department of Pharmaceutics  
Utrecht Institute for Pharmaceutical Sciences (UIPS)  
Utrecht University  
Utrecht 3512 JE, The Netherlands

K. Nazmi, F. J. Bikker  
Department of Oral Biochemistry  
Academic Center for Dentistry Amsterdam (ACTA)  
Amsterdam 1081 LA, The Netherlands

E. J. A. Veldhuizen  
Department of Biomolecular Health Sciences  
Division of Infectious Diseases and Immunology  
Faculty of Veterinary Medicine  
Utrecht University  
Utrecht 3584 CL, The Netherlands

P. Gonugunta, P. R. Anusuyadevi, P. Taheri  
Materials Science and Engineering Department (MSE)  
Faculty of Mechanical  
Maritime and Materials Engineering (3mE)  
Delft University of Technology  
Delft 2628 CD, The Netherlands

 The ORCID identification number(s) for the author(s) of this article can be found under <https://doi.org/10.1002/admt.202300500>

© 2023 The Authors. Advanced Materials Technologies published by Wiley-VCH GmbH. This is an open access article under the terms of the Creative Commons Attribution License, which permits use, distribution and reproduction in any medium, provided the original work is properly cited.

DOI: 10.1002/admt.202300500

Antibacterial coatings on surfaces are one of the most promising approaches for preventing biofilm formation.<sup>[6]</sup> In fact, local delivery of antibiotics can reduce the overuse of antibiotics in systemic antibiotic therapy (such as the treatment of chronic osteomyelitis) while increasing their effectiveness.<sup>[7]</sup> Nevertheless, the widespread use of antibiotics has resulted in the development of antibiotic-resistant bacteria, limiting the efficacy of coatings that are based on antibiotics.<sup>[8]</sup> Alternatively, some non-antibiotic compounds including host defense peptides (HDPs),<sup>[9]</sup> inorganic nanoparticles (e.g., copper, silver, etc.),<sup>[10]</sup> immunomodulatory agents (e.g. Interferon- $\gamma$  (IFN- $\gamma$ ))<sup>[11]</sup> and sphingoid bases<sup>[12]</sup> have been reported to have antimicrobial activity and could therefore be applicable for the development of antimicrobial coatings. Among novel antibacterial agents, HDPs (LL-37, Nisin, Magainin, etc.) are a group of antimicrobial peptides (AMPs) found in all organisms, including humans, that play a key role in the innate immune response and are able to overcome the resistance of certain antibiotic-resistant strains of bacteria,<sup>[13]</sup> making them potent candidate compounds for the development of antimicrobial coatings. Though, recent studies have revealed some challenges associated with the use of HDPs in the development of antibacterial coatings. As an example, due to their high minimum inhibitory concentration (MIC), a huge amount of peptides is needed in the coating, making them an impractical option from a financial perspective.<sup>[14]</sup> It should be noted that some groups have already attempted to use low concentrations of peptide, however they have only achieved 60% or 85% antibacterial efficacy,<sup>[15,16]</sup> which is considerably below the minimum clinical bactericidal properties (at least two logarithmic differences when compared to the control group). Additionally, HDP-based coatings do not possess long-lasting antibacterial properties due to the degradation or denaturation of the peptide in the physiological environment.<sup>[17]</sup>

Cationic and amphipathic CATH-2, also known as chicken cathelicidin-2, is a type of HDPs that belongs to the cathelicidin family. It is rich in arginine and lysine and has both immunomodulatory and strong antibacterial activity against a range of Gram-positive and Gram-negative bacteria.<sup>[18]</sup> It is not inactivated at serum or high salt concentrations.<sup>[19]</sup> In addition to the antibacterial agent, the type of material used for coating plays an instrumental role in the bio-stability and efficacy of the antibacterial coating.<sup>[20]</sup> Poly (D, L-lactide-co-glycolide) copolymers (PDLG) and gelatin methacryloyl (GelMA) are biodegradable, and biocompatible polymers. It is common to use these polymers in the formulation of drug delivery systems, including surface coatings, tissue engineering, and implantable devices.<sup>[21,22]</sup> Since PDLG polymers are biodegradable, they will gradually break down by enzymes or hydrolysis processes in the body, so there

will be no need for second surgery to remove the device.<sup>[23]</sup> Furthermore, GelMA is also biodegradable, and the degradation rate can be controlled by changing the crosslinking time and polymer concentration.<sup>[24]</sup> The electro spray method is extremely versatile when applying polymeric-based coatings, such as PDLG and GelMA. During the process, a polymer solution is created, and then an electric field is applied to the solution to create very fine particles.<sup>[25]</sup> It provides a high degree of control over coating thickness and produces uniform coatings. Moreover, this method has low costs, is relatively simple, and can be easily scaled up for industrial use.<sup>[26]</sup>

In this study, titanium (Ti) surfaces were electro sprayed with CATH-2 peptide using the layer-by-layer (LbL) assembly method<sup>[27]</sup> and release time and antibacterial activity were optimized for Ti implant coatings, without compromising host cells viability.

## 2. Results and Discussions

### 2.1. Surface Characterization

After HCl acid treatment of the Ti substrate, the surface roughness was increased (**Figure 1a**). The PDLG coating exhibited distributed pores in all coated groups, **Figure 1a,b**. It was observed that the PDLG coating in the [PDLG/-/-] and groups was uniform on the Ti surface, with an average coating thickness of approximately  $96.1 \pm 1.5 \mu\text{m}$ . The [PDLG/CA/-/], [PDLG/-/Gel], and [PDLG/CA/Gel] coatings had a comparable coating thickness of  $97.2 \pm 0.4$ ,  $98.2 \pm 0.8$ , and  $101.5 \pm 1.1 \mu\text{m}$ , respectively. Furthermore, some parts of the GelMA coating were diffused within the PDLG coating (**Figure 1b**).

The Attenuated Total Reflectance-Fourier Transform Infrared Spectroscopy (ATR-FTIR) spectra of [PDLG/-/-] and [PDLG/-/Gel] confirm the presence of PDLG and GelMA polymers, respectively. In the spectra of groups [PDLG/-/-], [PDLG/CA/-/], the stretching vibration region of functional groups containing C = N, C = C, and C = O falls within the  $1000\text{--}1800 \text{ cm}^{-1}$  wave number range. However, in [PDLG/CA/-] compared to [PDLG/-/-], the spectra band at  $1750 \text{ cm}^{-1}$  corresponding to the C = O bond was sharper. The  $800\text{--}600 \text{ cm}^{-1}$  wave number region corresponds to the IR stretching vibration region of functional groups containing C-Cl and C-C. Moreover, stretching bands caused by symmetric C-C(=O) vibrations were observed in the  $1300\text{--}1150 \text{ cm}^{-1}$  range (**Figure 1c**).<sup>[28]</sup> However, the unetched and etched Ti samples was not IR active. In the groups [PDLG/-/Gel] and [PDLG/CA/Gel], the spectra demonstrated characteristic peaks of the GelMA polymer. The N-H and O-H stretching vibrations are typically assigned to the absorption band around  $3346 \text{ cm}^{-1}$ , while the peaks in the range of  $2800\text{--}3100 \text{ cm}^{-1}$  are attributed to the C-H stretching vibration. GelMA's backbone structure is linked to absorption bands at  $1640 \text{ cm}^{-1}$  (amide I, C = O stretching),  $1500 \text{ cm}^{-1}$  (amide II, N-H bending coupled with C-H stretching), and  $1253 \text{ cm}^{-1}$  (amide III, C-N stretching and N-H bending). Notably, the peak around  $1640 \text{ cm}^{-1}$  in the GelMA spectrum, which corresponds to the C = C stretching of methacrylate groups, is situated too close to the amide I C = O stretching peak (**Figure 1c**).<sup>[29,30]</sup> Overall, the ATR-FTIR analysis indicated successfully implementing of coatings layer.

H. Weinans  
Biomechanical Engineering Department (BME)  
Faculty of Mechanical  
Maritime and Materials Engineering (3mE)  
Delft University of Technology  
Delft 2628 CD, The Netherlands  
S. Amin Yavari  
Regenerative Medicine Centre Utrecht  
Utrecht University  
Utrecht 3508 GA, The Netherlands

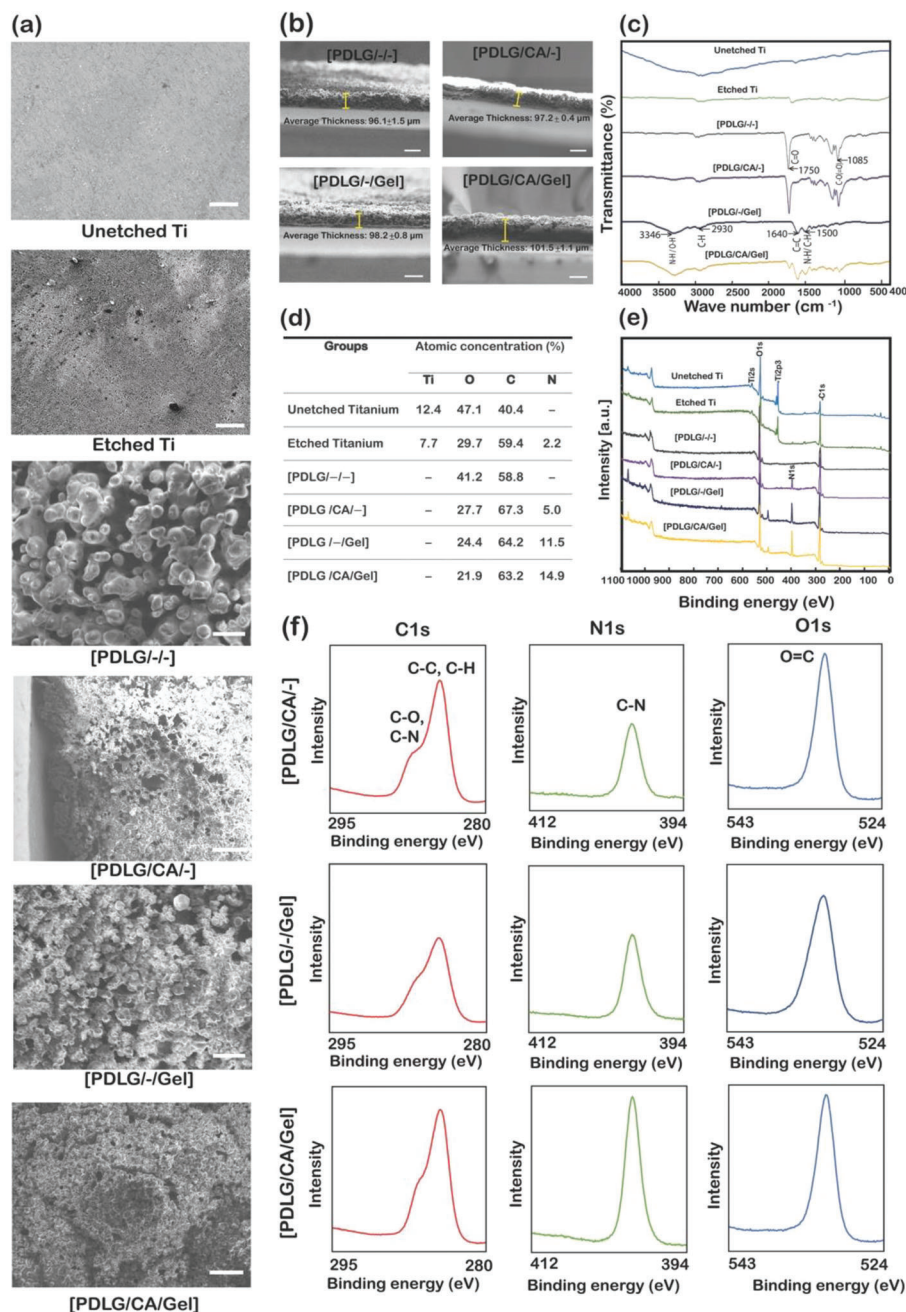


**Figure 1.** Surface characterization of uncoated and coated titanium implants. Scanning electron microscopy of a) surfaces morphology of unetched and etched titanium, [PDLG/-/-], [PDLG/CA/-], [PDLG/-Gel] and [PDLG/CA/Gel] groups and b) cross section view of coated implant, [PDLG/-/-], [PDLG/CA/-], [PDLG/-Gel] and [PDLG/CA/Gel], to determine coating thickness. c) Attenuated Total Reflectance-Fourier Transform Infrared Spectroscopy from the implant surfaces of unetched and etched titanium, [PDLG/-/-], [PDLG/CA/-], [PDLG/-Gel] and [PDLG/CA/Gel] groups in the wavenumber range of 400–4000  $\text{cm}^{-1}$  to provides and confirm of presence or absence of specific functional group. Atomic Low resolution x-ray photoelectron spectroscopy (XPS) d) to determine titanium, oxygen, carbon and nitrogen atomic concentration and e) binding energy surface of unetched and etched titanium, [PDLG/-/-], [PDLG/CA/-], [PDLG/-Gel] and [PDLG/CA/Gel] groups. f) High-resolution XPS spectra for C 1s, N 1s and O 1s peaks in [PDLG/CA/-], [PDLG/-Gel] and [PDLG/CA/Gel]. The scale bar of all images shows 100  $\mu\text{m}$ .

Additionally, X-ray photoelectron spectroscopy (XPS) was utilized to investigate the surface chemistry of the different samples. As illustrated in Figure 1d,e, three characteristic signals of Ti, C, and O were observed from both unetched and etched Ti substrates. The presence of the C element indicated environ-

mental carbon contamination. After electrospinning PDLG, the group [PDLG/-/-] exhibited two signals of O and C. The groups [PDLG/CA/-], [PDLG/-Gel], and [PDLG/CA/Gel] exhibited three signals of O, C, and N; with the intensity of N being less in the group without GelMA. Furthermore, the surface elemental



composition (Figure 1d) demonstrated that carbon and nitrogen atomic concentrations increased upon the deposition of GelMA and peptide coatings for all samples, while the oxygen atomic concentration decreased. The titanium and oxygen atomic concentrations decreased after HCl treatment. Following treatment and coating procedures, the Ti atomic concentration dropped from 7.7% to 0%. The high-resolution spectra of C1s, N1s and O1s for [PDLG/CA/-], [PDLG/-/Gel] and [PDLG/CA/Gel] are represented in Figure 1f and was further confirming that coating has been successfully applied.<sup>[31-34]</sup>

## 2.2. Coating Characterization and Stability

The effect of PDLG, peptide, and GelMA coating layers on Ti surface properties was evaluated using contact angle (CA) measurements. The etched Ti group demonstrated a lower CA value than the unetched Ti and displayed more hydrophilic behavior. This is due to the roughness created by etching. However, subsequent deposition of PDLG as a hydrophobic polymer on etched Ti increased the hydrophobicity and CA value. Furthermore, the addition of GelMA [PDLG/-/Gel] and peptide layer [PDLG/CA/-], improved the hydrophilicity of the coating, which decreased CA value (Figure 2a,b).

The CATH-2 release profile of [PDLG/CA/-] on day 1 shown releasing all CATH-2 (Figure 2c). An initial burst release of peptide was observed from the coating in group [PDLG/CA/Gel] on the first day followed by additional sustained releases on days 2, 3 and 4. In total, 75 µg of CATH-2 was released over 7 days. The proposed mechanism of action for peptide release includes diffusion through GelMA coating and degradation is illustrated in Figure 2d.

To determine the GelMA concentration following incubation, the degradation rate of GelMA in groups [PDLG/CA/Gel] and [PDLG/-/Gel] was analyzed using a BCA kit assay. Both groups indicated GelMA demonstrated a rapid degradation profile with a high release rate on the first day. It also demonstrated slow degradation on the following days. Quantitatively, more than 60% of GelMA was degraded after 1 day and almost 80% after 7 days in both groups (Figure 2e).

The mechanical shear resistance of a coating on Ti rod implants was qualitatively evaluated through implantation of a coated implant in a cadaveric rat bone. Upon examination, no evidence of coating delamination was observed on coated-etched Ti. The coating on unetched Ti was detached in some parts. The bone had to be broken to retrieve the implants, indicating their firm fixation (Figure 2f). To quantify the resistance of the [PDLG/CA/Gel] coating to mechanical forces during implantation, the weight loss of the coating after removal from the cadaveric bone was investigated. The results showed an average 5% and 40% weight loss of coating on etched and unetched Ti, respectively (Figure S2, Supporting Information).

## 2.3. Antibacterial Properties

CATH-2 peptide antibacterial mechanism on both Gram-positive and Gram-negative was illustrated (Figure 3a). The colony-forming units (CFU) counting of the collected release media

against planktonic *S. aureus* and *E. coli* bacteria over a period of 5 days were used to determine the antibacterial activity. As presented in Figure 3b,c on day 1, all groups with peptide in coatings had no live planktonic bacteria. [PDLG/CA/Gel] killed 100% of bacteria for 4 days, while the [PDLG/CA/-] group did not exhibit any antimicrobial properties. The collected released media of all groups on day 5 was demonstrated no antibacterial activity. Furthermore, the CFU counting of sonicated implants showed [PDLG/CA/Gel] coatings completely eradicated the bacteria on day 4 and was not allowed adherent bacteria either positive or negative strain to grow on the implant (Figure 3d,e).

To verify the bactericidal properties of the coatings, the bacteria treated with the implants, after being incubated for 4 days in PBS, were stained and analyzed using confocal laser scanning microscopy (CLSM, Leica SP8X, Germany). The images revealed that in both positive and negative strains, the surfaces of the specimens from the Ti, [PDLG/-/-], [PDLG/CA/-], and [PDLG/-/Gel] groups were associated with the accumulation of live bacteria (green dots). On the other hand, the surfaces of the specimens containing both peptide and GelMA, [PDLG/CA/Gel] group, had no live bacteria, and all bacteria being dead (red dots) (Figure 3f,g). CLMS images confirmed the quantitative CFU assay results.

## 2.4. Cell Viability

The cytocompatibility and cellular adhesion of human mesenchymal stem cells (hMSCs) and macrophage cell lines to the surfaces of the samples were evaluated over 7 days. As presented in Figure 4a, the viability of hMSCs on the implants was confirmed using a quantitative AlamarBlue assay. Results showed a steady increase in total metabolic activity over 7 days for all groups when compared to blank specimens. However, for the macrophage cell line, the cell viability of the [PDLG/CA/-] group was significantly reduced compared to the other groups at days 1, 3, and 7 (Figure 4b). Using a qualitative live-dead assay on day 7, it was found that hMSCs adhered and spread homogeneously on all implants and no dead cells (red stain) were observed on the implants cultured with hMSCs (Figure 4c). In comparison to other groups, a higher number of dead cells was observed on the [PDLG/CA/-] sample, while all the macrophage cells in the other groups were live (Figure 4d).

## 2.5. Discussion

In this study, we determined the biocompatible concentration of the antibacterial CATH-2 peptide. We found that it could be effectively loaded onto Ti substrates using the LbL coating method. Specifically, the Ti surface was first etched with 37% HCl and then coated with PDLG. This was followed by adding 80 µg CATH-2 peptide and applying a GelMA layer to form an LbL coating. The electrospray method was used to apply both PDLG and GelMA to achieve efficient peptide loading and durable LbL coating. The resulting peptide-coated Ti samples exhibited strong antibacterial activity against both Gram-positive and Gram-negative bacteria and were biocompatible with hMSCs and macrophage cells. Therefore, local delivery of CATH-2 at sufficiently high

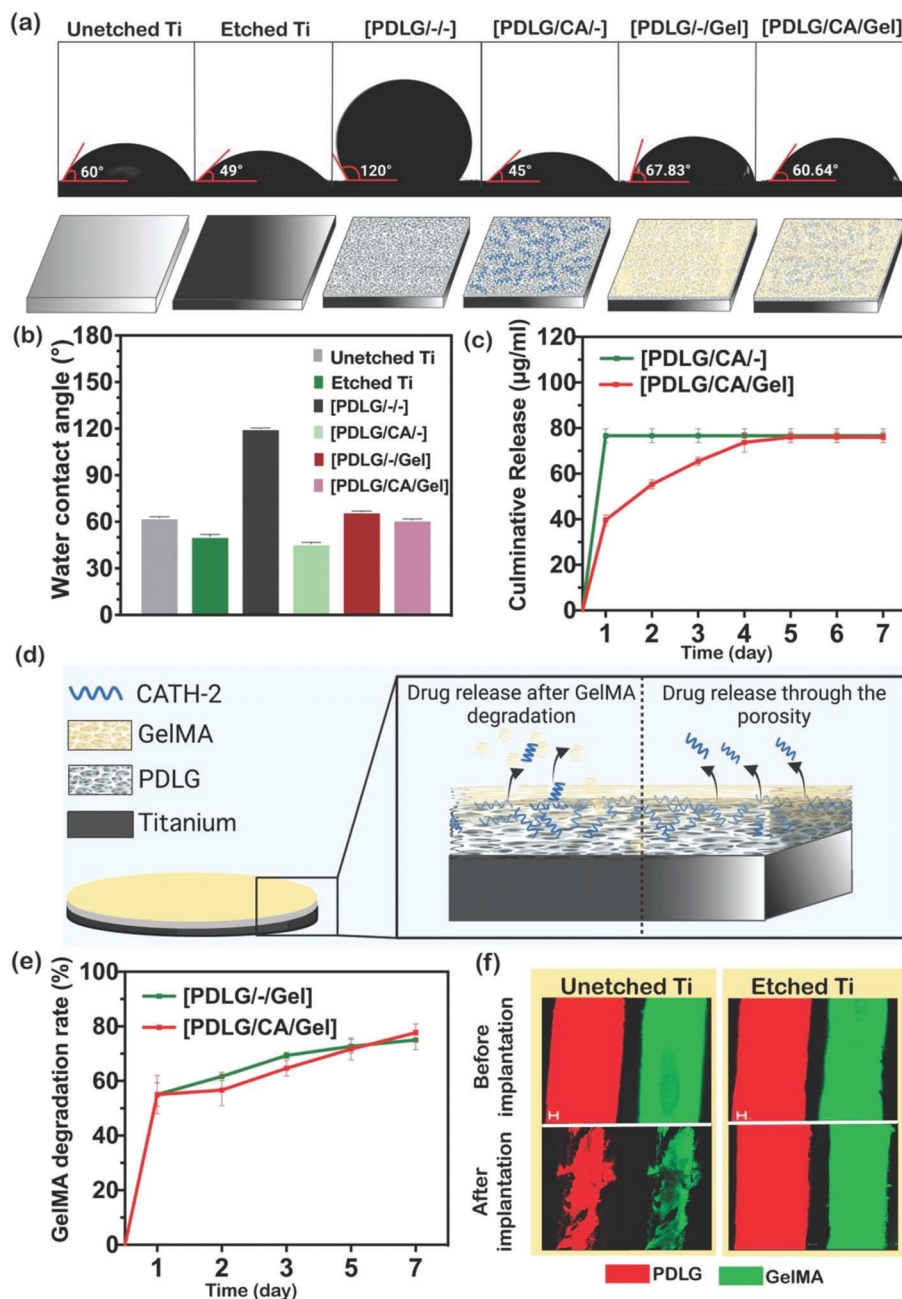


**Figure 2.** a) Optical images of the water contact angle of unetched and etched titanium, [PDLG/-/-], [PDLG/CA/-], [PDLG/-/Gel] and [PDLG/CA/Gel] groups to determine the wettability. Schematic illustrates different surface structures (created by BioRender.com). b) The water contact angle measurement on the surface. The uncertainty of the contact angle measurements was determined from the standard deviation of 3 independent measurements. c) Cumulative release profile of CATH-2 conjugated-Tamara at an excitation wavelength of 550–590 nm from [PDLG/CA/Gel] samples for 7 days using multiplate reader. d) Schematic presents CATH-2 release mechanisms from LbL coating in group [PDLG/CA/Gel] (created by BioRender.com). e) Release profile of GelMA degradation from [PDLG/CA/Gel] samples over one week via BCA kit assay. f) CLSM imaging before and after press-fit implantation of the unetched and etched titanium implant in a cadaveric rat bone, coated with PDLG/GelMA labeled with Nile-red (red) and FITC (green), respectively. Data represent the means  $\pm$  SD ( $n = 3$ ) and the scale bar shows 100  $\mu$ m.

concentrations is capable of eradicating residual bacteria. To prevent bacteria spread from the implant surface to the surrounding tissue and to eradicate bacteria contaminating tissue during surgery, a rapid initial release of antimicrobial agents followed by a sustained release is necessary.

The surface morphologies and corresponding coating thickness measurements of the samples are shown in Figure 1a,b. Acid treatment improved the polymer coating's adhesion to the Ti surface. By creating many acid-etched pits, the surface became rougher which resulted in more efficient polymer coating

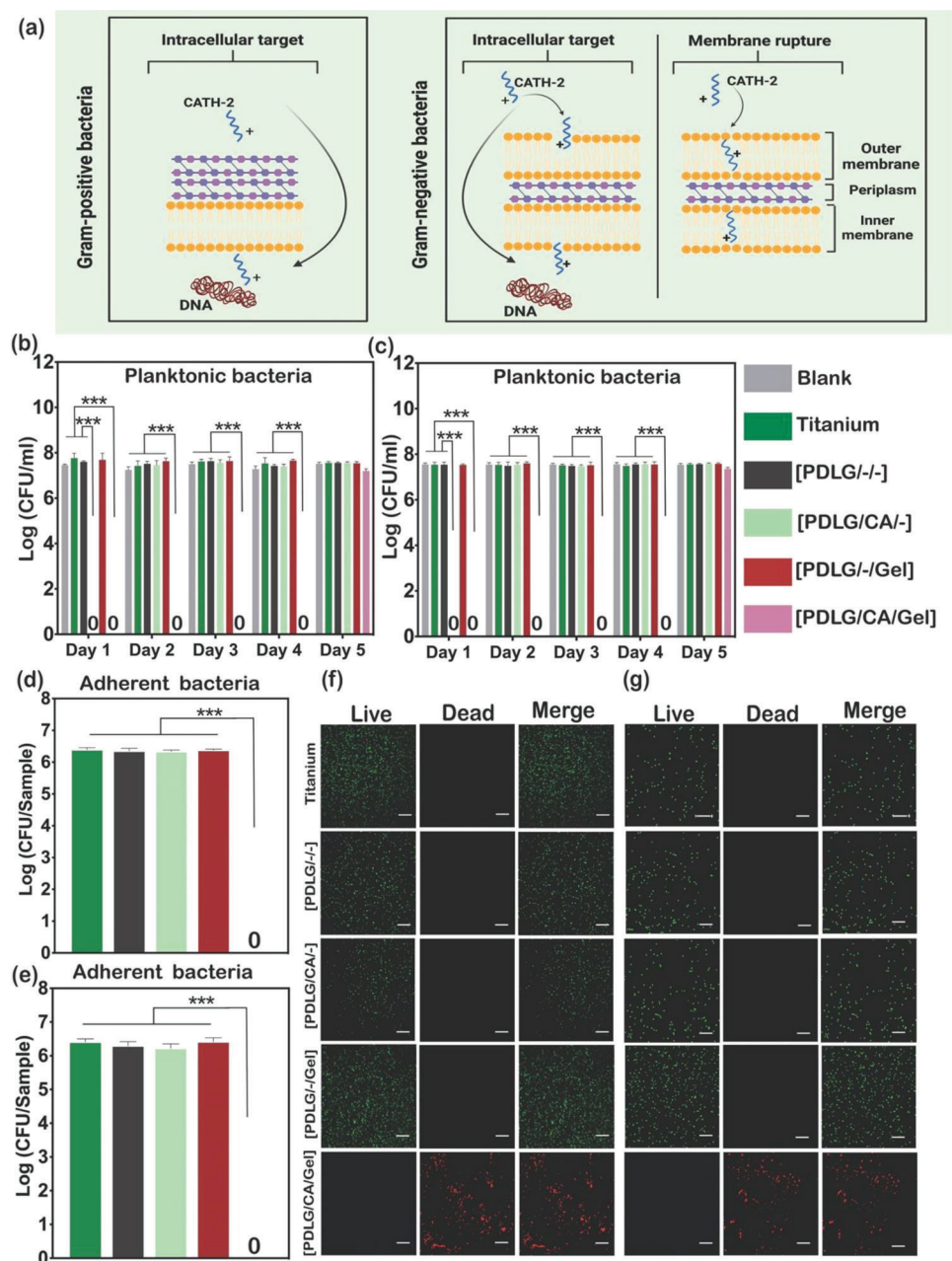


**Figure 3.** Antibacterial activity of etched titanium, [PDLG/-/-], [PDLG/CA/-], [PDLG/-Gel] and [PDLG/CA/Gel] groups. a) Schematic represents the antibacterial mechanism of CATH-2 peptide against both gram-negative and gram-positive bacteria (created by Biorender.com). Colony forming unit (CFU) of the implant's collected supernatant incubated in PBS over 5 days against b) *S. aureus* and c) *E. coli*. CFU of samples after incubation 4 days in PBS and sonicated to measure adherent d) *S. aureus* and e) *E. coli* bacteria on implants. Live-dead assay of adherent bacteria on specimens after incubation 4 days in PBS and sonication to visualize (e) *S. aureus* and (f) *E. coli* bacteria by confocal laser scanning microscopy. The green and red dots represent live and dead bacteria, respectively. Data shows the means  $\pm$  SD ( $n = 3$ ,  $*p < 0.05$ ;  $**p < 0.01$ ;  $***p < 0.001$ ) and the scale bar shows 100  $\mu$ m.

adhesion.<sup>[35]</sup> In addition, this process can also remove any contaminants on the Ti surface that may interfere with the adhesion of the polymer coating. This ensures a strong and durable bond between Ti and the coating.<sup>[36]</sup> Through the electro spray technique developed in this study, PDLG and GelMA coatings were uniformly applied to the implant. The coatings showed distributed pores in all coated groups. By electro spraying fine droplets of a polymer solution, the solvent evaporated, leaving

behind a solid layer of polymer. The use of electro spray in the coating process can result in the formation of a porous structure within the coating, which can be distributed across the surface.<sup>[37]</sup> Furthermore, electro spray coating allowed CATH-2 embedded in the porosity of PDLG coating to be preserved. It improved GelMA coating's adhesion to Ti substrates while preserving the CATH-2 embedded within the PDLG. Besides, the study presented in this paper investigated the coating characteristics by ATR-FTIR



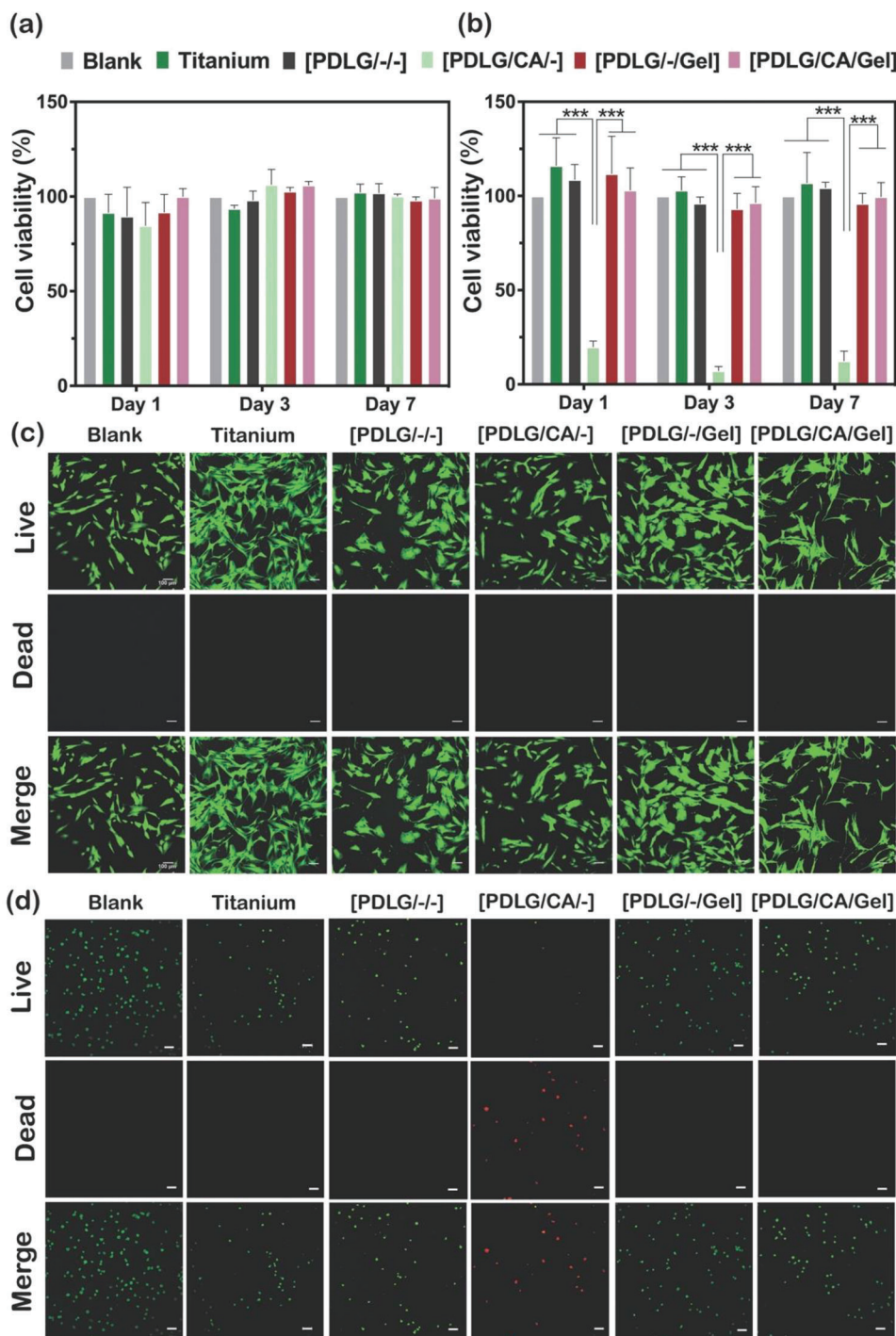


**Figure 4.** Cytotoxicity of etched titanium, [PDLG/-/-], [PDLG/CA/-], [PDLG/-/Gel] and [PDLG/CA/Gel] groups. AlamarBlue activity assay of implants for different time points of 1, 3 and 7 days cultured with a) human mesenchymal stem cells (hMSCs) and b) macrophage cell line. Live-dead assay on day 7 by confocal laser scanning microscopy of sample's surface cultured by c) hMSCs and d) macrophage cell line. Data represent the means  $\pm$  SD ( $n = 3$ ,  $*p < 0.05$ ;  $**p < 0.01$ ;  $***p < 0.001$ ) and the scale bar shows 100  $\mu\text{m}$ .

and low and high resolution XPS of different coatings applied to Ti substrates (Figure 1c,e,f). These analyses provided valuable information about the surface chemical composition and bond of uncoated and coated substrates. They also helped to understand the interaction between the coating and the substrate,

which can further improve the coating process. The ATR-FTIR spectra of the coated groups confirmed the presence of PDLG, GelMA, and peptide. XPS analysis demonstrated an increase in carbon and nitrogen atomic concentrations upon the deposition of GelMA and peptide coatings. In contrast, the oxygen atomic



concentration decreased. The results suggest that the coating process on Ti substrates has been successful. The CA measurements indicated that the addition of CATH-2 and GelMA coating layers increased the CA value, which suggests that the coatings have hydrophilic properties. Hydrophilic coatings can improve cell adhesion and proliferation by promoting the adsorption of proteins and other biological molecules.<sup>[38]</sup> Coating thickness and uniformity can be carefully controlled, so that the drugs can be released precisely. At body temperature, GelMA degraded, and CATH-2 was released. By adjusting the GelMA polymer's chemical composition and crosslinking density, drug release and degradation can be fully controlled and tuned.<sup>[39]</sup>

A kinetic model named First-order kinetic yielded the most accurate fit for observed release kinetics. This model can be used to describe water-soluble drugs dissolution within porous matrixes or barrier membrane coatings, indicating that the system is concentration-dependent, and that degradation-diffusion is likely to be the mechanism by which CATH-2 is released.<sup>[40,41]</sup> Illustrative CATH-2 release and GelMA degradation are depicted schematically (Figure 2d). It showed that GelMA degradation increased the pore size of the protective layer enabling peptide release. When GelMA is exposed to PBS suspension, it swells, causing drug diffusion. The outermost surface of the GelMA layer, representing the diffusion zone, was expected to play a primary role in initial burst release of CATH-2.<sup>[42]</sup> A drug's release rate can also be influenced by its solubility, which impacts its diffusion rate.<sup>[43]</sup> Also, the rapid initial release of antibacterial drug is effective in killing all bacteria which is crucial as the local immune defenses may be impaired after implantation, leaving the implant vulnerable to bacterial colonization on the implant surface and delayed release of drug may allow bacteria to infiltrate host cells.<sup>[44,45]</sup> It was observed that the LbL coating exhibited a high initial CATH-2 release rate, followed by a sustained slow release. A sustained antimicrobial effect administered over a prolonged period is necessary to prevent the development of bacterial colonies and biofilm formation.<sup>[46]</sup> The [PDLG/CA/Gel] demonstrated effective antimicrobial activity against *S. aureus* and *E. coli* bacteria in vitro for 4 days without cytotoxicity to hMSCs and macrophage cells. As such, the current LbL coating resulted in high drug delivery efficacy in a bactericidal concentration without cytotoxic side effects. GelMA, as an outer layer, is an ideal substrate for host cell adhesion and proliferation. This makes it a suitable candidate for applications as a coating for bone implants.<sup>[47,48]</sup>

It is also crucial that the bone implants coating remains intact and functional throughout surgery. An antibacterial coating should retain its effectiveness over a longer time period, producing the desired therapeutic effects.<sup>[20,49]</sup> The etching process on Ti implants can enhance the adhesion of the PDLG and GelMA coating to the Ti substrate and thereby increase the stability of the final coating, which can be attributed to the strong bond between the implant and the electro-sprayed coating (Figure 2f). Moreover, there are many factors that can affect the mechanical stability of a GelMA coating, including its degree of crosslinking, substrate, GelMA concentration and any additional components like the applied incorporated drugs or cross-linker component.<sup>[50,51]</sup>

When the cathelicidin peptide comes into contact with bacteria, the carboxy-terminal domain of it is cleaved off.<sup>[52]</sup> Studies have demonstrated that the likelihood of antibacterial resis-

tance developing against CATH-2 is minimal, which is crucial. It has the ability to combat antimicrobial-resistant bacteria without provoking significant resistance.<sup>[53]</sup> Moreover, CATH-2 has been shown to be a potent inhibitor and eradicator of biofilms.<sup>[54]</sup> CATH-2 possesses a proline residue at its center, which destabilizes its helical conformation and may influence how it interacts with biological membranes. As a result of CATH-2's net positive charge and amphipathicity, it interacts strongly with lipopolysaccharide (LPS) and inner membranes, resulting in cell lysis, self-uptake, or the formation of pores, which facilitate further penetration (Figure 3a).<sup>[55–57]</sup> CATH-2 binding to LPS does not appear antimicrobial directly. It is more likely that LPS in the outer membrane serves as a barrier that the peptide must overcome before reaching its target. This could be the cytoplasmic membrane or an intracellular target, or both.<sup>[55]</sup> Bacterial membranes wrinkle and fragment when exposed to CATH-2. CATH-2 has been shown to have bactericidal effects on *E. coli* and demonstrated that it has distinct effects on Gram-negative bacterial membranes and intracellular contents.<sup>[56]</sup> It binds via hydrogen bonding, but also exhibits hydrophobic binding at higher concentrations. Hydrophobic interactions between peptide and membrane can disrupt membrane.<sup>[58]</sup> In the interaction between CATH-2 and Gram-positive bacteria, membrane perturbation was observed in *S. aureus* as a result of the interaction with negatively charged surface molecules, such as lipoteichoic acid (LTA) and cardiolipin, resulting in the formation of lamellar mesosomes and membrane permeabilization.<sup>[57]</sup>

Peptides that destabilize bacterial membranes may also affect human cell membranes. However, a coating containing antimicrobial properties should not exhibit significant cytotoxicity to mammalian cells.<sup>[59]</sup> While cationic HDP can rapidly permeabilize prokaryotic membranes, most natural peptides are relatively less toxic to eukaryotic cells. LL-37 and CATH-2 can enter eukaryotic cells and facilitate nucleic acids and DNA dye entry without cell lysis. This phenomenon is cell-type dependent, with primary human lymphocytes and monocytes relatively unaffected by high CATH-2 peptide concentrations.<sup>[60]</sup> Our results indicate no measurable toxicity against hMSCs and a human macrophage cell line for CATH-2 when efficiently coated on a Ti substrate.

Peptide-based antibacterial coatings face some challenges, including coating preparation and drug delivery, as well as high production costs.<sup>[59,60]</sup> CATH-2 displays broad antimicrobial activity and exerts strong immunomodulatory effects, including binding to LPS, neutralization of the immune response, and enhancement of DNA-induced activation of Toll-like receptor 21 (TLR21).<sup>[61,62]</sup> In this study, antibacterial activity and cytotoxicity were separately checked. However, the co-culture model can simultaneously evaluate the immunomodulatory and antibacterial activity of the compound by incubating it with immune cells and bacteria and measuring changes in cytokine production and bacterial growth, respectively.<sup>[63]</sup> Future studies should aim to address the limitations of current antibacterial peptide coatings that may enhance their efficacy against a wide range of bacteria, particularly against biofilm-forming strains. Additionally, it would be worthwhile to investigate the potential for bacterial resistance to these peptide coatings, and develop strategies to mitigate this risk. In spite of numerous publications on peptide-based antibacterial coatings, only a few studies have been performed in vivo, which is essential for their clinical application.

Finally, the PDLG/GelMA coating can serve as a multipurpose delivery platform for administering antibacterial peptides safely and without causing harm to cells. It could be particularly useful in addressing infections related to bone implants. By utilizing multiple GelMA coatings, it is possible to improve drug release longevity and load multiple drugs. Further research could be done to optimize drug release kinetics. This will ensure that the coating provides a sustained release of antibacterial peptides over a prolonged period of time.

### 3. Experimental Section/Methods

#### 3.1. Peptide Synthesis

The CATH-2 peptide (RFGRFLRKIRRFKPKVTITIQGSARF-NH) and fluorescent CATH-2 conjugated-Tamra dye were synthesized by Fmoc-chemistry at the Academic Centre for Dentistry Amsterdam (Amsterdam, the Netherlands). By using solid phase peptide synthesis using fluoren-9-ylmethoxycarbonyl (Fmoc) protected amino acids (OrpegenPharma GmbH, Heidelberg, Germany) and (Novabiochem, Darmstadt, Germany) in a Syro II synthesizer (Biotage, Uppsala Sweden). Labeling of CAHT-2 with 5,6-carboxytetramethylrhodamine (TAMRA), (Iris Biotech GmbH, Marktredwitz, Germany) was carried out in-synthesis using an additional Fmoc-Ahx-OH (NovaBiochem) at the N-terminus. CAHT-2 peptide and the TAMRA-labeled were purified to a purity of at least 95% by preparative RP-HPLC UltiMate 3000 Series (Thermo scientific, Massachusetts USA) on Vydac C18 column (218MS510, Vydac, Hesperia, CA, USA) and the authenticity of the CAHT-2 and TMRA labeled peptide was confirmed by MALDI-TOF mass spectrometry on a Microflex LRF mass spectrometer equipped with an additional gridless reflector (Burker Daltonic, Bremen, Germany).

#### 3.2. Layer by Layer Coating

Ti disks (Alfa Aeser by Thermo Fisher Scientific, US), 6.0 mm in diameter and 0.25 mm in thickness, were treated with concentrated hydrochloric acid HCl 37% (Merk, Germany) at 60 °C for 30 min, and disks were immersed and washed with distilled water and dried in the oven at 40 °C for 1 h (Etched Ti).<sup>[64]</sup> After surface modification, the disks were ultrasonically cleaned with acetone, ethanol and distilled water each for 10 min, and then allowed to air dry. The Ti disks were coated with a multi-layer coating through sequential layering, resulting in multiple layers on top of each other. To coat Ti implants, PDLG (50:50, Thermo Fisher Scientific, US) was dissolved in trifluoroethanol (TFE, Sigma-Aldrich, Germany) at a concentration of 50 mg mL<sup>-1</sup> for 2 h at room temperature. A 0.5 mL h<sup>-1</sup> flow rate was employed, and a sample distance of 100 mm was used to electrocoat the prepared solution for 120 min. In order to generate particles, an electric field (16 kV) was applied with a high voltage power supply (Heinzinger LNC 30000, Germany). CATH-2 was loaded onto samples by dissolving it in deionized water (Milli-Q) to a concentration of 2g L<sup>-1</sup>. 40 µL of CATH-2 solution was pipetted onto the PDLG-coated samples. Peptides were spread out slightly and dried at room temperature for 1 h. PDLG coating was controlled by fixing the coating weight at 5 mg per implant.

**Table 1.** An overview of all experimental groups' specifications.

Group's name	PDLG (mg per implant)	CATH-2 (µg per implant)	GelMA (mg per implant)
Etched titanium (Ti)	—	—	—
Etched titanium + PDLG Coating ((PDLG/-/-))	5	—	—
Etched titanium + PDLG coating + CATH-2 ((PDLG/CA/-))	5	80	—
Etched titanium + PDLG coating + GelMA coating ((PDLG/-/Gel))	5	—	2
Etched titanium + PDLG coating + CATH-2 + GelMA coating ((PDLG/CA/Gel))	5	80	2

GelMA was synthesized using previously established methods.<sup>[22]</sup> Briefly, 10% w/v porcine type A gelatin (Merk, US) was dissolved in phosphate-buffered saline (PBS, Thermo Fisher Scientific, US) at 50°C while stirring continuously. A solution of Methacrylic anhydride (60% w/v, Merk, US) was added to the gelatin solution. A pH adjustment was made using 5 mM sodium hydroxide (NaOH) after the reaction was terminated with 3x PBS, and excess methacrylic Anhydride was centrifuged at 4000 rpm to remove excess. After dialyzing with Milli-Q water for 5 days at 4 °C, the solution was filtered through 0.2 µm pores and lyophilized to sterilize it.

A final concentration of 3% GelMA was achieved at room temperature by gently mixing it with Milli-Q water. After this, 0.5% Irgacure (Merk, US) was added to the solution. Electrospray conditions were the same as those described for the PDLG layer, where the solution was loaded into a syringe and electrocoated at a spray rate of 0.5 mL h<sup>-1</sup> for 90 min. After coating, samples were exposed to UV-irradiation (Bluepoint ecocure, Germany) for 1 min to form a stable hydrogel coating. The GelMA coating was adjusted by of 2 mg per implant. Briefly, four additional control groups were established where no coating was present on Ti, where the CATH-2 and GelMA were not present, but PDLG was present [PDLG/-/-], where the CATH-2 and PDLG layer were present, but the GelMA layer was absent [PDLG/CA/-], and where PDLG and GelMA were loaded without peptide [PDLG/-/Gel]. Etched Ti was used to prepare all of the different groups. **Table 1** summarizes the specifications of all experimental groups.

#### 3.3. Surface Characterization

The coatings morphology was examined using field emission scanning electron microscopy (FESEM, JEOL, JSM-6500F). Prior to measurements, the samples were carbon sputtered for 25 s, resulting in a thickness of around 17.8 nm, using JEOL-JEC-530 auto carbon coater equipment, to ensure the conductivity of the samples. Representative images of the coated specimens were selected by inspecting several regions of the implant surface quasi-randomly. The inspected areas displayed different morphologies, and images showing some recurrent patterns were chosen as representative images. To measure the overall thickness of the

coatings, half-coated samples were tilted by FESEM and cross-section images were taken. After importing these images into ImageJ software, the coatings thickness was measured quantitatively by measuring its height across multiple regions of the image. This allowed for an average thickness measurement that accounted for any thickness variations across the coating surface.

The coating surface chemistry was characterized using XPS. Here, analyses were carried out using a PHI-TFA XPS spectrometer (Physical Electronic Inc.), equipped with an x-ray Al1 K $\alpha$  X-ray monochromatic source ( $h\nu = 1486.7$  eV). The vacuum during the XPS analysis was maintained around  $10^{-9}$  mbar and the pass energy during survey was 89.45 eV. During measurements, the diameter of the analyzed circular area was 0.4 mm, and the corresponding depth of analysis was 3–5 nm. Narrow multiplex scans of C1s, O1s and N1s peaks were collected in high resolution mode with pass energies of 71.55 eV. They had resolution of 0.2 eV, at a 45° take-off angle. The acquired spectra were processed using MultiPak v.8.0 (Physical Electronics Inc.), for curve fitting and atomic concentrations calculation.

The chemical structures of the coated surfaces were analyzed using ATR-FTIR (Perkin Elmer Instruments, US). The transmittance spectra of the coated samples were recorded in the wavenumber range of 400–4000  $\text{cm}^{-1}$ . The samples were mounted on the sample stage and placed in contact with an ATR crystal.

In order to determine the CA of different surfaces, the sessile drop method was used. Digital cameras were connected to optical microscopes to measure CA values and SCA20 software (Data physics instrument Company, Filderstadt, Germany) was used to analyze them. Three measurements were done on each sample, and the average value was reported.

### 3.4. Coating Characterization and Stability

#### 3.4.1. CATH-2 Release Profile

Fluoroskan Ascent FL multiplate reader (Thermo LabSystems, Finland) was used to measure the fluorescent signal generated by CATH-2 conjugated-Tamra at an excitation wavelength of 550–590 nm to determine the peptide release profile. The [PDLG/CA/Gel] samples were incubated in 1 mL of PBS (pH 7.4) at 37 °C for 7 days, and the media containing the peptide was collected and replaced daily. The concentration of CATH-2 in the samples at various time points was measured to calculate cumulative release profiles. In order to determine the cumulative release curves, a titration of CATH-2 conjugated to Tamra as a standard was prepared.

#### 3.4.2. GelMA Degradation

The degradation of the GelMA hydrogel in the groups of [PDLG-/Gel] and [PDLG/CA/Gel] was evaluated by incubating the samples in PBS for 7 days. The samples were placed in 200  $\mu\text{L}$  PBS at pH 7.4 and the media was collected and refreshed daily. The concentration of degraded GelMA in PBS was determined using the BCA kit assay (Thermo Fisher, US) as per the manufacturer's protocol. The degradation rate was calculated by normalizing the

concentration of degraded GelMA at the indicated time points to the total GelMA content.

#### 3.4.3. Coating Durability

Rod-shaped Ti implant (RatFix Shoulder screw, RSystem, Switzerland), with a length of 6.5 mm and a diameter of 0.8 mm was used. The ability of the coatings to withstand surgical implantation in the group [PDLG/CA/Gel] was evaluated by implanting unetched and etched Ti coated with 5 mg Nile-red (Thermo Fisher Scientific, US) loaded PDLG and 2 mg FITC-loaded GelMA into cadaveric rat tibiae with a surgical procedure, previously reported.<sup>[65]</sup> The coatings were visualized before and after implantation by CLSM. To quantify the amount of coating remaining after explanation, the explanted implants were washed with demineralized water to remove any tissue residue, dried completely and weighed. The coating weight loss was calculated using Equation 1. Where  $w_0$  represents the initial weight of the coating before implantation and  $w_1$  represents the final weight after washing and drying.

$$\text{weight loss(\%)} = \frac{w_0 - w_1}{w_0} \quad (1)$$

### 3.5. Antibacterial Activity

#### 3.5.1. Bacterial Culture

The antibacterial activity of the coating was assessed using green fluorescent protein (GFP) labelled *S. aureus* (strain: SH1000) and *E. coli* (strain: MG1655). These bacteria were transformed with a GFP-expressing plasmid pCM29 to facilitate constitutive GFP expression, as per established protocols.<sup>[66,67]</sup> *S. aureus* was grown in Todd-Hewitt broth (THB) containing 10  $\mu\text{g mL}^{-1}$  chloramphenicol at 37 °C for 16 h to reach stationary phase. The overnight bacterial culture was then diluted in THB to achieve a final inoculum concentration of  $10^6$  CFU  $\text{mL}^{-1}$ . Similarly, *E. coli* was prepared in Luria-Bertani broth medium without chloramphenicol.

#### 3.5.2. Antibacterial Assay

The coated samples were incubated at 37 °C in PBS for 5 days. Culture media were collected daily and refreshed. The collected release media in 48-well plate was then exposed to the 1 mL prepared bacterial suspension. The plates were incubated at 37 °C in an incubator for 16 h before counting CFU for each plate. The number of planktonic bacteria was quantified by CFU assay in serial dilutions of the bacterial suspension.

For the quantification of the adherent bacteria on implant on day 4, the implants kept in PBS at 37 °C for 4 days. After discarding the supernatant, the implants were incubated with mixing of 1 mL prepared bacteria and fresh PBS at 37 °C for 16 h. The samples were rinsed three times with PBS and then sonicated for 1 min in 1 mL fresh PBS. The supernatant was used for CFU determination using the same method as mentioned.

Furthermore, the implants exposed to the GFP-labelled bacterial suspension, as mentioned above, were analyzed by CLSM following staining with SYTOX Orange Nucleic Acid Stain (Thermo

Fisher Scientific, US). Specifically, the 20  $\mu\text{L}$  SYTOX orange solution (50  $\mu\text{M}$  stock concentration) was added to the suspension of overnight incubated implants with bacteria and was kept with the dye-solution for 15 min at room temperature. Images were acquired using CLSM at a magnification of 20x. The fluorescence signals emitted by live cells (green, with an excitation wavelength range of 396–508 nm) and dead cells (red, with an excitation wavelength range of 547–570 nm) were analyzed and processed using software provided by the CLSM manufacturer (Leica software).

### 3.6. Cytotoxicity

#### 3.6.1. hMSCs Isolation and Culture

In accordance with institutional medical ethics committee approval and written informed consent obtained from patients, bone marrow samples were collected from three individuals who underwent orthopedic surgery at the University Medical Center Utrecht in the Netherlands under the protocols METC 08-001/K and METC 07-125/C. The mononuclear cell fraction was obtained through Ficoll-Paque centrifugation, and subsequently cultured in growth medium composed of minimum essential medium supplemented with 100 units  $\text{mL}^{-1}$  Penicillin-Streptomycin antibiotics (Pen-Strep, Thermo Fisher Scientific, US) and 10% fetal bovine serum (FBS, Invitrogen, UK) for 48 h. The plastic-adherent cells were then expanded to passage 5. These hMSCs were then seeded onto implants in 48-well plate at a density of 10,000 cells per 500  $\mu\text{L}$  and were maintained in a humidified incubator (37  $^{\circ}\text{C}$ , 5%  $\text{CO}_2$ ). Every third day of the culture period, the medium was replaced.

#### 3.6.2. Monocyte (THP-1) Isolation and Culture

An in vitro model of macrophage polarization was previously described, utilizing THP-1 monocytes (ATCC, Teddington, UK) as a starting population, which were differentiated into macrophages through exposure to Phorbol 12-myristate 13-acetate (PMA).<sup>[68]</sup>

Briefly, the human monocytic leukemia cell line THP-1 was cultured in RPMI 1640 culture medium (Thermo Fisher Scientific, US) supplemented with 10% v/v FBS and 1% v/v Pen-Strep at 37  $^{\circ}\text{C}$  in 5%  $\text{CO}_2$  in a humidified incubator for 1 day. To induce differentiation, PMA (Sigma-Aldrich, Germany) was added to a final concentration of 100 nM. After 2 days, the PMA supplemented media was removed, and the cells were washed with PBS and allowed to rest for an additional 24 h in fresh PMA-free media to acquire macrophages. These cells were cultured onto samples in 48-well plates at a density of 5,000 cells per 500  $\mu\text{L}$  and were maintained in a humidified incubator (37  $^{\circ}\text{C}$ , 5%  $\text{CO}_2$ ). Every third day of the culture period, the medium was replaced.

#### 3.6.3. Cell Viability Assay

To investigate the impact of CATH-2 release from the coating on host cells' behavior, five groups of implants were incubated with cells for 7 days. First, the coated implants were sterilized for 1 h

with ultraviolet radiation. The macrophage and hMSCs cells were seeded into the coated implants in a 48-well plate at a density of 5,000 and 10,000 cells per well in growth medium, respectively. The cytotoxicity of all implants was evaluated with the Alamar blue metabolic activity assay at different timepoints (days 1, 3 and 7) by incubation with 10% Alamar Blue Cell Viability Reagent (Thermo Scientific, USA) in growth medium. The fluorescence signal at 540–590 nm was read using a multiplate reader after 3 h. Fluorescence values of blank samples (untreated cells) were considered 100% viable. Before calculating the percentage of cell viability, the background signal from wells containing only AlamarBlue reagent was subtracted. In addition, other experimental groups were normalized compared to blank samples.

Cell adhesion and survival were evaluated using a live/dead cell viability staining kit (Thermo Scientific, US) as per the manufacturer's instructions on day 7. The samples were then analyzed using CLSM. Fluorescence signals from live cells (green, 500–525 nm) and dead cells (red, 528–640 nm) were processed and analyzed with Leica software.

### 3.7. Statistical Analysis

Data are presented as mean  $\pm$  standard deviation and sample size was 3 ( $n = 3$ ). A one-way ANOVA followed by Tukey post-hoc correction was used for comparison of group means in SPSS (version 26, IBM SPSS statistics). The Shapiro-Wilk test was employed to assess data normality. A P value of 0.05 was used as a threshold for statistical significance. \* $p < 0.05$ ; \*\* $p < 0.01$ ; \*\*\* $p < 0.001$ .

## 4. Conclusions

In conclusion, the study demonstrated the successful use of antibacterial CATH-2 peptide in a LbL coating method. This was for the development of antibacterial coatings on Ti substrate. The electrospray method was used to apply PDLG and GelMA coatings to achieve efficient peptide loading and a durable coating. The resulting peptide-coated titanium samples exhibited strong antibacterial activity against both *S. aureus* and *E. coli* bacteria and were biocompatible with hMSCs and macrophage cells. The use of GelMA allowed for a prolonged release of CATH-2, which effectively prevented bacterial adhesion to titanium implants without compromising host cells viability. Degradation-diffusion is likely the mechanism by which CATH-2 is released. The study provides a promising approach to developing antibacterial coatings for use in the prevention of biofilm formation and the treatment of bone implant related infection.

## Supporting Information

Supporting Information is available from the Wiley Online Library or from the author.

## Acknowledgements

This publication is part of the project DARTBAC (with project number NWA.1292.19.354) of the research program NWA-ORC which is (partly) financed by the Dutch Research Council (NWO). The kind support of Dr. Azin Khodaei, Dr. Alireza Hassani, Leonardo Cecotto and Nada Rahmani in running the experiment is appreciated.



## Conflict of Interest

The authors declare no conflict of interest.

## Data Availability Statement

The data that support the findings of this study are available from the corresponding author upon reasonable request.

## Keywords

antibacterial peptides, antibiotic resistance, biomaterial-related infection, durable coatings

Received: March 30, 2023

Revised: July 12, 2023

Published online: August 2, 2023

- [1] S. A. Yavari, S. M. Castenmiller, J. A. G. van Strijp, M. S. C. A. Yavari, M. Croes, S. M. Castenmiller, J. A. G. van Strijp, *Adv. Mater.* **2020**, *32*, 2002962.
- [2] J. A. Inzana, E. M. Schwarz, S. L. Kates, H. A. Awad, *Biomaterials* **2016**, *81*, 58.
- [3] D. Lopez, I. Leach, E. R. Moore, A. Norrish, *Indian J Orthop* **2017**, *51*, 397.
- [4] M. H. Abdul-Aziz, K. Brady, M. O. Cotta, J. A. Roberts, *Ther Drug Monit* **2022**, *44*, 19.
- [5] D. Sharma, L. Misba, A. U. Khan, *Antimicrob Resist Infect Control* **2019**, *8*, 76.
- [6] A. Uneputti, A. Dávila-Lezama, D. Garibo, A. Oknianska, N. Bogdanchikova, J. F. Hernández-Sánchez, A. Susarrey-Arce, *Colloid Interface Sci. Commun.* **2022**, *46*, 100560.
- [7] E. A. Masters, R. P. Trombetta, K. L. de Mesy Bentley, B. F. Boyce, A. L. Gill, S. R. Gill, K. Nishitani, M. Ishikawa, Y. Morita, H. Ito, S. N. Bello-Irizarry, M. Ninomiya, J. D. Brodell, C. C. Lee, S. P. Hao, I. Oh, C. Xie, H. A. Awad, J. L. Daiss, J. R. Owen, S. L. Kates, E. M. Schwarz, G. Muthukrishnan, *Bone Res.* **2019**, *7*, 20.
- [8] P. P. Kalkar, M. Riddick, A. J. García, *Nat. Rev. Mater.* **2021**, *7*, 39.
- [9] Y. Qian, S. Deng, X. Wu, Y. She, R. Liu, H. Lin, *J. Mater. Sci. Technol.* **2021**, *91*, 90.
- [10] S. Raza, K. Matuła, S. Karoń, J. Paczesny, *Antibiotics* **2021**, *10*, 435.
- [11] L. E. DeForge, K. L. Billeci, S. M. Kramer, *J. Immunol. Methods* **2000**, *245*, 79.
- [12] F. J. Bikker, M. A. Hoogenkamp, A. Malhaoui, K. Nazmi, J. Neilands, B. P. Krom, *Caries Res* **2018**, *52*, 7.
- [13] E. Sun, C. R. Belanger, E. F. Haney, R. E. W. Hancock, in *Peptide Applications in Biomedicine, Biotechnology and Bioengineering*, Elsevier, Cambridge, MA **2018**, pp. 253–285.
- [14] M. Kazemzadeh-Narbat, H. Cheng, R. Chabok, M. M. Alvarez, C. de la Fuente-Nunez, K. S. Phillips, A. Khademhosseini, *Crit. Rev. Biotechnol.* **2020**, *41*, 94.
- [15] N. Y. Pfeufer, K. Hofmann-Peiker, M. Mühle, P. H. Warnke, M. C. Weigel, M. Kleine, *J. Bone Jt. Surg* **2011**, *93*, 840.
- [16] P. Cao, K. Liu, X. Liu, W. Sun, D. Wu, C. Yuan, X. Bai, C. Zhang, *Colloids Surf., B.* **2020**, *194*, 111198.
- [17] S. S. Griesser, M. Jasieniak, K. Vasilev, H. J. Griesser, *Coatings* **2021**, *11*, 68.
- [18] A. Van Dijk, M. Van Eldik, E. J. A. Veldhuizen, H. L. M. Tjeerdsma-Van Bokhoven, M. R. De Zoete, F. J. Bikker, H. P. Haagsman, *PLoS One* **2016**, *11*, 0147919.
- [19] V. A. F. Schneider, M. Coorens, S. R. Ordonez, J. L. M. Tjeerdsma-Van Bokhoven, G. Posthuma, A. Van Dijk, H. P. Haagsman, E. J. A. Veldhuizen, *Sci. Rep.* **2016**, *6*, 1.
- [20] M. Cloutier, D. Mantovani, F. Rosei, *Trends Biotechnol.* **2015**, *33*, 637.
- [21] S. A. Yehia, A. H. Elshafeey, I. Elsayed, *J. Liposomes Res.* **2012**, *22*, 128.
- [22] K. Yue, G. Trujillo-de Santiago, M. M. Alvarez, A. Tamayol, N. Annabi, A. Khademhosseini, *Biomaterials* **2015**, *73*, 254.
- [23] H. Azevedo, R. Reis, *Biodegrad. Syst. Tissue Eng. Regener. Med.* **2005**.
- [24] Y. Piao, H. You, T. Xu, H. P. Bei, I. Z. Piwko, Y. Y. Kwan, X. Zhao, *Eng. Regeneration* **2021**, *2*, 47.
- [25] J. R. Smith, D. A. Lamprou, C. Larson, S. J. Upson, *Trans. IMF* **2021**, *100*, 25.
- [26] A. Reale, L. LaNotte, L. Salamandra, G. Polino, G. Susanna, T. M. Brown, F. Brunetti, A. DiCarlo, *Energy Technol.* **2015**, *3*, 385.
- [27] P. Gentile, I. Carmagnola, T. Nardo, V. Chiono, *Nanotechnology* **2015**, *26*, 422001.
- [28] T. Kaur, R. Kaur, A. Kaur, *Pharm. Sci.* **2014**, *2*, 30.
- [29] D. F. S. Fonseca, P. C. Costa, I. F. Almeida, P. Dias-Pereira, I. Correia-Sá, V. Bastos, H. Oliveira, C. Vilela, A. J. D. Silvestre, C. S. R. Freire, *Macromol. Biosci.* **2020**, *20*, 2000195.
- [30] Y. Yan, Y. Cao, R. Cheng, Z. Shen, Y. Zhao, Y. Zhang, G. Zhou, S. Sang, *Tissue Eng Regen Med* **2022**, *19*, 59.
- [31] S. Zanini, C. Riccardi, A. Natalello, G. Cappelletti, D. Cartelli, F. Fenili, A. Manfredi, E. Ranucci, *Mater. Res. Exp.* **2014**, *1*, 035001.
- [32] B. Lu, X. Lv, Y. Le, *Polymers* **2019**, *11*, 304.
- [33] J. Du, Y. Yao, M. Wang, R. Su, X. Li, J. Yu, B. Ding, *Adv. Funct. Mater.* **2022**, *32*, 2109833.
- [34] G. Tan, L. Zhou, C. Ning, Y. Tan, G. Ni, J. Liao, P. Yu, X. Chen, *Appl. Surf. Sci.* **2013**, *279*, 293.
- [35] A. Jemat, M. J. Ghazali, M. Razali, Y. Otsuka, *BioMed. Res. Int.* **2015**, *2015*, 791725.
- [36] H. Chouirfa, H. Bouloussa, V. Migonney, C. Falentin-Daudré, *Acta Biomater.* **2019**, *83*, 37.
- [37] S. Zhang, C. Campagne, F. Salaün, *Appl. Sci.* **2019**, *9*, 402.
- [38] L. C. Xu, C. A. Siedlecki, *Biomaterials* **2007**, *28*, 3273.
- [39] H. Samadian, H. Maleki, Z. Allahyari, M. Jaymand, *Coord. Chem. Rev.* **2020**, *420*, 213432.
- [40] S. Garg, K. Pathak, A. Philip, D. Puri, *Sci. Pharm.* **2012**, *80*, 229.
- [41] M. Kazemzadeh-Narbat, B. F. L. Lai, C. Ding, J. N. Kizhakkedathu, R. E. W. Hancock, R. Wang, *Biomaterials* **2013**, *34*, 5969.
- [42] Z. Q. Zhao, B. L. Zhang, H. Q. Chu, L. Liang, B. Z. Chen, H. Zheng, X. D. Guo, *Biomater Adv* **2022**, *133*, 112620.
- [43] P. Borgquist, A. Körner, L. Piculell, A. Larsson, A. Axelsson, *J. Controlled Release* **2006**, *113*, 216.
- [44] S. A. J. Zaat, *Biomaterials Associated Infection: Immunological Aspects and Antimicrobial Strategies*, Springer Science+Business Media, New York **2013**, p. 175.
- [45] M. Riool, A. de Breij, J. W. Drijfhout, P. H. Nibbering, S. A. J. Zaat, *Front Chem.* **2017**, *5*, 63.
- [46] P. Gao, X. Nie, M. Zou, Y. Shi, G. Cheng, *J. Antibiot.* **2011**, *64*, 625.
- [47] E. Choi, D. Kim, D. Kang, G. H. Yang, B. Jung, M. G. Yeo, M. J. Park, S. H. An, K. H. Lee, J. S. Kim, J. C. Kim, W. Jeong, H. H. Yoo, H. Jeon, *Regen Biomater.* **2021**, *8*, 1.
- [48] Y. Xiang, W. Wang, Y. Gao, J. Zhang, J. Zhang, Z. Bai, S. Zhang, Y. Yang, *Front Bioeng Biotechnol* **2020**, *8*, 971.
- [49] S. Hügl, V. Scheper, M. M. Gepp, T. Lenarz, T. S. Rau, J. Schwieger, *J. Mech Behav Biomed Mater* **2019**, *97*, 90.
- [50] M. Sun, X. Sun, Z. Wang, S. Guo, G. Yu, H. Yang, *Polymers* **2018**, *10*, 1290.
- [51] M. Y. Shie, J. J. Lee, C. C. Ho, S. Y. Yen, H. Y. Ng, Y. W. Chen, *Polymers* **2020**, *12*, 1930.
- [52] W. Gao, L. Xing, P. Qu, T. Tan, N. Yang, D. Li, H. Chen, X. Feng, *Sci. Rep.* **2015**, *5*, 1.
- [53] E. J. A. Veldhuizen, E. C. Brouwer, V. A. F. Schneider, A. C. Fluit, *PLoS One* **2013**, *8*, e61964.

- [54] H. Chen, R. W. Wubbolts, H. P. Haagsman, E. J. A. Veldhuizen, *Sci. Rep.* **2018**, *8*, 10446.
- [55] P. Sharma, S. Sharma, S. Joshi, P. Barman, A. Bhatt, M. Maan, N. Singla, P. Rishi, M. E. Ali, S. Preet, A. Saini, *Sci. Rep.* **2022**, *12*, 1.
- [56] V. A. F. Schneider, M. Coorens, S. R. Ordonez, J. L. M. Tjeerdsma-Van Bokhoven, G. Posthuma, A. Van Dijk, H. P. Haagsman, E. J. A. Veldhuizen, *Sci. Rep.* **2016**, *6*, 32948.
- [57] V. A. F. Schneider, M. Coorens, J. L. M. T. Bokhoven, G. Posthuma, A. van Dijk, E. J. A. Veldhuizen, H. P. Haagsman, *mSphere* **2017**, *2*, e00370.
- [58] M. R. Scheenstra, M. van den Belt, J. L. M. Tjeerdsma-van Bokhoven, V. A. F. Schneider, S. R. Ordonez, A. van Dijk, E. J. A. Veldhuizen, H. P. Haagsman, *Sci. Rep.* **2019**, *9*, 4780.
- [59] W. Aoki, M. Ueda, *Pharmaceuticals* **2013**, *6*, 1055.
- [60] N. Mookherjee, M. A. Anderson, H. P. Haagsman, D. J. Davidson, *Nat. Rev. Drug Discovery* **2020**, *19*, 311.
- [61] M. Coorens, A. van Dijk, F. Bikker, E. J. A. Veldhuizen, H. P. Haagsman, *J. Immunol.* **2015**, *195*, 3970.
- [62] M. Coorens, V. A. F. Schneider, A. M. de Groot, A. van Dijk, M. Meijerink, J. M. Wells, M. R. Scheenstra, E. J. A. Veldhuizen, H. P. Haagsman, *J. Immunol.* **2017**, *199*, 1418.
- [63] L. Cecotto, K. van Kessel, M. A. Wolfert, C. Vogely, B. van der Wal, H. Weinans, J. van Strijp, S. Amin Yavari, *iScience* **2022**, *25*.
- [64] A. S. Diab Al-Radha, *IOSR-JDMS* **2016**, *15*, 87.
- [65] M. Croes, S. Bakhshandeh, I. A. J. van Hengel, K. Lietaert, K. P. M. van Kessel, B. Pouran, B. C. H. van der Wal, H. C. Vogely, W. Van Hecke, A. C. Fluit, C. H. E. Boel, J. Alblas, A. A. Zadpoor, H. Weinans, S. Amin Yavari, *Acta Biomater.* **2018**, *81*, 315.
- [66] D. A. Heesterbeek, B. W. Bardoel, E. S. Parsons, I. Bennett, M. Ruyken, D. J. Doorduijn, R. D. Gorham, E. T. Berends, A. L. Pyne, B. W. Hoogenboom, S. H. Rooijackers, *EMBO J.* **2019**, *38*, 99852.
- [67] E. Boero, I. Brinkman, T. Juliet, E. van Yperen, J. A. G. van Strijp, S. H. M. Rooijackers, K. P. M. van Kessel, *Front. Immunol.* **2021**, *12*, 38.
- [68] M. Genin, F. Clement, A. Fattaccioli, M. Raes, C. Michiels, *BMC Cancer* **2015**, *15*, 577.